Nonlinear dynamics of two-color optical vortices in lithium niobate crystals

Alexander Dreischuh[1,2], Dragomir N. Neshev[1], Vesselin Z. Kolev[3], Solomon Saltiel[1,2], Marek Samoc[3], Wieslaw Krolikowski[3], and Yuri S. Kivshar[1]

[1]*Nonlinear Physics Center, Research School of Physical Sciences and Engineering, Australian National University, Canberra ACT 0200, Australia*
[2]*Department of Quantum Electronics, Faculty of Physics, Sofia University, Bulgaria*
[3]*Laser Physics Center, Research School of Physical Sciences and Engineering, Australian National University, Canberra ACT 0200, Australia*

Abstract: We study experimentally the nonlinear dynamics of two-color optical vortex beams in the presence of second-harmonic generation combined with the effects of photo- and thermal refraction, as well as self- and induced-phase modulation. We use an iron-doped lithium niobate crystal as a nonlinear medium for the vortex propagation and observe experimentally, depending on the laser wavelength, a decay of a double-charge vortex, splitting and reshaping of background beam, pattern formation, and controllable nonlinear rotation of a vortex pair.

OCIS codes: (190.4420), Nonlinear optics, transverse effects in; (190.0190), Nonlinear optics; (190.5330), Photorefractive nonlinear optics; (190.2620), Frequency conversion; (190.5940) Self-action effects.

References and links

1. D. G. Grier, "A revolution in optical manipulation," Nature **424,** 810–816 (2003).
2. G. Foo, D. M. Palacios, and G. A. Swartzlander, "Optical vortex coronagraph," Opt. Lett. **30,** 3308–3310 (2005).
3. S. Furhapter, A. Jesacher, S. Bernet, and M. Ritsch Marte, "Spiral interferometry," Opt. Lett. **30,** 1953–1955 (2005).
4. G. Molina Terriza, J. P. Torres, and L. Torner, "Twisted photons," Nature Physics **3,** 305–310 (2007).
5. L. Allen, M. J. Padgett, and M. Babiker, "The orbital angular momentum of light," Prog. Opt. **39**, 291–372 (1999).
6. M. S. Soskin and M. V. Vasnetsov, "Singular optics," Prog. Opt. **42**, 219–276 (2001).
7. A. S. Desyatnikov, Yu. S. Kivshar, and L. Torner, "Optical vortices and vortex solitons," Prog. Opt. **47**, 291–391 (2005).
8. W. J. Firth and D. V. Skryabin, "Optical solitons carrying orbital angular momentum," Phys. Rev. Lett. **79,** 2450–2453 (1997).
9. D. V. Skryabin and W. J. Firth, "Dynamics of self-trapped beams with phase dislocation in saturable Kerr and quadratic nonlinear media," Phys. Rev. E **58,** 3916–3930 (1998).
10. L. Torner and D. V. Petrov, "Azimuthal instabilities and self-breaking of beams into sets of solitons in bulk second-harmonic generation," Electron. Lett. **33,** 608–610 (1997).
11. L. T. Vuong, T. D. Grow, A. Ishaaya, A. L. Gaeta, G. W. Hooft, 't, E. R. Eliel, and G. Fibich, "Collapse of optical vortices," Phys. Rev. Lett. **96,** 133901–4 (2006).
12. V. Tikhonenko, J. Christou, and B. Luther-Davies, "Spiraling bright spatial solitons formed by the breakup of an optical vortex in a saturable self-focusing medium," J. Opt. Soc. Am. B **12,** 2046–2052 (1995).
13. Yu. S. Kivshar and B. Luther-Davies, "Dark optical solitons: physics and applications," Phys. Rep. **298,** 81–197 (1998).
14. Yu. S. Kivshar and G. P. Agrawal, *Optical Solitons: From Fibers to Photonic Crystals* (Academic Press, San Diego, 2003).
15. D. Rozas, Z. S. Sacks, and G. A. Swartzlander, "Experimental observation of fluidlike motion of optical vortices," Phys. Rev. Lett. **79,** 3399–3402 (1997).

#91939 - $15.00 USD Received 22 Jan 2008; revised 31 Mar 2008; accepted 31 Mar 2008; published 3 Apr 2008

16. E. B. Sonin, "Vortex oscillations and hydrodynamics of rotating superfluids," Rev. Mod. Phys. **59,** 87–155 (1987).
17. D. Rozas, C. T. Law, and G. A. Swartzlander, "Propagation dynamics of optical vortices," J. Opt. Soc. Am. B **14,** 3054–3065 (1997).
18. D. Neshev, A. Dreischuh, M. Assa, and S. Dinev, "Motion control of ensembles of ordered optical vortices generated on finite extent background," Opt. Commun. **151,** 413–421 (1998).
19. G. Indebetouw, "Optical vortices and their propagation," J. Mod. Opt. **40,** 73–87 (1993).
20. F. S. Roux, "Dynamical behavior of optical vortices," J. Opt. Soc. Am. B **12,** 1215–1221 (1995).
21. Yu. S. Kivshar, J. Christou, V. Tikhonenko, B. Luther-Davies, and L. M. Pismen, "Dynamics of optical vortex solitons," Opt. Commun. **152,** 198–206 (1998).
22. G. H. Kim, H. J. Lee, L. U. Kim, and H. Suk, "Propagation dynamics of optical vortices with anisotropic phase profiles," J. Opt. Soc. Am. B **20,** 351–359 (2003).
23. J. Christou, V. Tikhonenko, Yu. S. Kivshar, and B. LutherDavies, "Vortex soliton motion and steering," Opt. Lett. **21,** 1649–1651 (1996).
24. B. Luther-Davies, R. Powles, and V. Tikhonenko, "Nonlinear rotation of 3-dimensional dark spatial solitons in a gaussian laser-beam," Opt. Lett. **19,** 1816–1818 (1994).
25. A. Berzanskis, A. Matijosius, A. Piskarskas, V. Smilgevicius, and A. Stabinis, "Conversion of topological charge of optical vortices in a parametric frequency converter," Opt. Commun. **140,** 273–276 (1997).
26. I. V. Basistiy, V. Y. Bazhenov, M. S. Soskin, and M. V. Vasnetsov, "Optics of light-beams with screw dislocations," Opt. Commun. **103,** 422–428 (1993).
27. K. Dholakia, N. B. Simpson, M. J. Padgett, and L. Allen, "Second-harmonic generation and the orbital angular momentum of light," Phys. Rev. A **54,** R3742–R3745 (1996).
28. M. S. Soskin and M. V. Vasnetsov, "Nonlinear singular optics," Pure Appl. Opt. **7,** 301–311 (1998).
29. A. Dreischuh, G. G. Paulus, F. Zacher, F. Grasbon, D. Neshev, and H. Walther, "Modulational instability of multiple-charged optical vortex solitons under saturation of the nonlinearity," Phys. Rev. E **60**, 7518–7524 (1999).
30. S. M. Saltiel, A. A. Sukhorukov, and Yu. S. Kivshar, "Multistep parametric processes in nonlinear optics" Prog. Opt. **47**, 1–73 (2005).
31. K. H. Yang, J. R. Morris, P. L. Richards, and Y. R. Shen, "Phase-matched far-infrared generation by optical mixing of dye laser beams," Appl. Phys. Lett. **23,** 669–671 (1973).
32. G. D. Miller, R. G. Batchko, W. M. Tulloch, D. R. Weise, M. M. Fejer, and R. L. Byer, "42%-efficient single-pass cw second-harmonic generation in periodically poled lithium niobate," Opt. Lett. **22,** 1834–1836 (1997).
33. K. Noguchi, O. Mitomi, and H. Miyazawa, "Millimeter-wave Ti : $LiNbO_3$ optical modulators," J. Lightwave Technol. **16,** 615–619 (1998).
34. G. C. Valley, M. Segev, B. Crosignani, A. Yariv, M. M. Fejer, and M. C. Bashaw, "Dark and bright photovoltaic spatial solitons," Phys. Rev. A **50,** R4457–R4460 (1994).
35. D. Runde, S. Brunken, C. E. Rutter, and D. Kip, "Integrated optical electric field sensor based on a Bragg grating in lithium niobate," Appl. Phys. B **86,** 91–95 (2007).
36. F. S. Chen, J. T. LaMacchia, and D. B. Fraser, "Holographic storage in lithium niobate," Appl. Phys. Lett. **13,** 223 (1968).
37. X. An, D. Psaltis, and G. W. Burr, "Thermal fixing of 10,000 holograms in $LiNbO_3$: Fe," Appl. Opt. **38,** 386–393 (1999).
38. D. N. Nikogosyan, *Properties of Optical and Laser-Related Materials: A Handbook* (Wiley, Chichester, UK, 1997).
39. L. Arizmendi, "Photonic applications of lithium niobate crystals," Phys. Status Solidi A **201,** 253–283 (2004).
40. F. Pettazzi, V. Coda, M. Chauvet, and E. Fazio, "Frequency-doubling in self-induced waveguides in lithium niobate," Opt. Commun. **272,** 238–241 (2007).
41. R. G. Batchko, M. M. Fejer, R. L. Byer, D. Woll, R. Wallenstein, V. Y. Shur, and L. Erman, "Continuous-wave quasi-phase-matched generation of 60 mW at 465 nm by single-pass frequency doubling of a laser diode in backswitch-poled lithium niobate," Opt. Lett. **24,** 1293–1295 (1999).
42. B. Crosignani, M. Segev, D. Engin, P. Diporto, A. Yariv, and G. Salamo, "Self-trapping of optical beams in photorefractive media," J. Opt. Soc. Am. B **10,** 446–453 (1993).
43. G. C. Valley, M. Segev, B. Crosignani, A. Yariv, M. M. Fejer, and M. C. Bashaw, "Dark and bright photovoltaic spatial solitons," Phys. Rev. A **50,** R4457–R4460 (1994).
44. M. Taya, M. C. Bashaw, M. M. Fejer, M. Segev, and G. C. Valley, "Observation of dark photovoltaic spatial solitons," Phys. Rev. A **52,** 3095–3100 (1995).
45. D. N. Neshev et al., "Nonlinear spectral-spatial control and localization of supercontinuum radiation," Phys. Rev. Lett. **99,** 123901–4 (2007).
46. Z. Chen, M. Segev, D. W. Wilson, R. E. Muller, and P. D. Maker, "Self-trapping of an optical vortex by use of the bulk photovoltaic effect," Phys. Rev. Lett. **78,** 2948–2951 (1997).
47. R. DeSalvo, A. A. Said, D. J. Hagan, E. W. Van Stryland, and M. SheikBahae, "Infrared to ultraviolet measurements of two-photon absorption and n(2) in wide bandgap solids," IEEE J. Quantum Electron. **32,** 1324–1333 (1996).
48. D. H. Jundt, M. M. Fejer, and R. L. Byer, "Optical-properties of lithium-rich lithium-niobate fabricated by vapor

#91939 - $15.00 USD Received 22 Jan 2008; revised 31 Mar 2008; accepted 31 Mar 2008; published 3 Apr 2008

transport equilibration," IEEE J. Quantum Electron. **26,** 135–138 (1990).
49. S. Lan, M. F. Shih, G. Mizell, J. A. Giordmaine, Z. G. Chen, C. Anastassiou, J. Martin, and M. Segev, "Second-harmonic generation in waveguides induced by photorefractive spatial solitons," Opt. Lett. **24,** 1145–1147 (1999).
50. A. D. Boardman, W. Ilecki, and Y. Liu, "Spatial solitons in a photorefractive medium sustaining second-harmonic generation," J. Opt. Soc. Am. B **19,** 832–838 (2002).
51. J. F. Reintjes, *Nonlinear Optical Parametric Processes in Liquids and Gasses* (Academic Press, New York, 1984).
52. S. Dinev and A. Dreischuh, "Sum-frequency generation in the xuv," Opt. Quantum Electron. **23,** 91–97 (1991).
53. A. Dreischuh, U. Reiter Domiaty, D. Gruber, L. Windholz, and S. Dinev, "Nonlinear alignment between conical emissions generated in a four-wave parametric mixing process," Appl. Phys. B **66,** 175–180 (1998).
54. M. F. Shih, Z. G. Chen, M. Mitchell, M. Segev, H. Lee, R. S. Feigelson, and J. P. Wilde, "Waveguides induced by photorefractive screening solitons," J. Opt. Soc. Am. B **14,** 3091–3101 (1997).
55. S. Lan, C. Anastassiou, M. Segev, M. Shih, J. A. Giordmaine, and G. Mizell, "Tuning of second-harmonic generation in waveguides induced by photorefractive spatial solitons," Appl. Phys. Lett. **77,** 2101–2103 (2000).
56. S. Orlov, A. Yariv, and M. Segev, "Nonlinear self-phase matching of optical second harmonic generation in lithium niobate," Appl. Phys. Lett. **68,** 1610–1612 (1996).
57. C. Lou, J. Xu, H. Qiao, X. Zhang, Y. Chen, and Z. Chen, "Enhanced second-harmonic generation by means of high-power confinement in a photovoltaic soliton-induced waveguide," Opt. Lett. **29,** 953–955 (2004).
58. A. E. Siegman, *Lasers* (University Science Books, Sausalito, Calif., 1986), p. 1283.
59. K. Bezuhanov, A. Dreischuh, G. G. Paulus, M. G. Schatzel, and H. Walther, "Vortices in femtosecond laser fields," Opt. Lett. **29,** 1942–1944 (2004).
60. K. Bezuhanov, A. Dreischuh, G. G. Paulus, M. G. Schatzel, H. Walther, D. Neshev, W. Krolikowski, and Y. Kivshar, "Spatial phase dislocations in femtosecond laser pulses," J. Opt. Soc. Am. B **23,** 26–35 (2006).
61. S. Szatmari, G. Kuhnle, and P. Simon, "Pulse-compression and traveling-wave excitation scheme using a single dispersive element," Appl. Opt. **29,** 5372–5379 (1990).
62. F. Grasbon, A. Dreischuh, G. G. Paulus, F. Zacher, and H. Walther, "Femtosecond interferometric autocorrelations in the presence of pulse front distortions," Proc. SPIE **3571,** 164–168 (1999).
63. G. A. Swartzlander and J. Schmit, "Temporal correlation vortices and topological dispersion," Phys. Rev. Lett. **93,** 093901–4 (2004).
64. SNLO nonlinear optics code available from A.V. Smith, Sandia National Laboratories, Albuquerque, NM87185-1423.
65. P. P. Ho, D. Ji, Q. Z. Wang, and R. R. Alfano, "Temporal behavior of cross-phase-modulated second-harmonic generation of ultrashort laser pulses in nonlinear-optical media," J. Opt. Soc. Am. B **7**, 276–284 (1990)
66. M. Horowitz, R. Daisy, O. Werner, and B. Fischer, "Large thermal nonlinearities and spatial self-phase modulation in $Sr_xBa_{1-x}Nb_2O_6$ and $BaTiO_3$ crystals," Opt. Lett. **17,** 475–477 (1992).
67. V. Z. Kolev, M. J. Lederer, B. Luther-Davies, and A. V. Rode, "Passive mode locking of a Nd:YVO_4 laser with an extra-long optical resonator," Opt. Lett. **28,** 1275–1277 (2003).
68. R. R. Alfano, P. L. Baldeck, P. P. Ho, and G. P. Agrawal, "Cross-phase modulation and induced focusing due to optical nonlinearities in optical fibers and bulk materials," J. Opt. Soc. Am. B **6,** 824–829 (1989).
69. I. W. Hsieh, X. G. Chen, J. I. Dadap, N. C. Panoiu, R. M. Osgood, S. J. Mcnab, and Y. A. Vlasov, "Cross-phase modulation-induced spectral and temporal effects on co-propagating femtosecond pulses in silicon photonic wires," Opt. Express **15,** 1135–1146 (2007), http://www.opticsinfobase.org/abstract.cfm?URI=oe-15-3-1135.
70. F. M. Mitschke and L. F. Mollenauer, "Discovery of the soliton self-frequency shift," Opt. Lett. **11,** 659–661 (1986).
71. J. P. Gordon, "Theory of the soliton self-frequency shift," Opt. Lett. **11,** 662–664 (1986).

1. Introduction

The study of optical vortices (OVs) has received a special attention in recent years due to a variety of potential applications of the vortex beams including particle micro-manipulation [1], imaging [2], interferometry [3], and quantum information [4]. An optical vortex is associated with a light beam whose phase varies in a screw-type way around an isolated singular point. This characteristic helical phase of an OV is described by the multiplier $\exp(im\theta)$, where θ is the azimuthal coordinate, and the integer number m stands for the vortex topological charge. The helical phase results in a non-zero orbital angular momentum of the light beam [5, 6] which strength depends on the vortex charge.

The optical vortices are associated with doughnut beams or Laguerre-Gaussian (LG) modes. As such they are eigenmodes of the free-space equation and propagate without any change of their shape. However, in nonlinear media the vortex propagation is affected by the beam induced change of the refractive index as well as by the phase and index gradients induced

#91939 - $15.00 USD Received 22 Jan 2008; revised 31 Mar 2008; accepted 31 Mar 2008; published 3 Apr 2008

by other beams [7]. While in nonlinear media with the self-focusing nonlinearity the vortex beam becomes unstable due to the azimuthal modulational instability [8, 9, 10, 11, 12], in self-defocusing media a doughnut beam can form a dark vortex soliton with a strongly localized self-trapped vortex core [7, 13, 14]. Analogously to point vortices in fluid dynamics [15, 16], optical vortices of the same charge with localized cores orbit each other at the rate which is inversely proportional to the squared vortex separation distance [17, 18]. The nonlinearity of the material, being the key for manipulation of the vortex dynamics [17, 19, 20, 21, 22], can alter dramatically this type of the vortex fluid-like motion, including the vortex steering [23] and the rotation of a vortex pair [18, 24].

One of the important nonlinear processes which affects strongly the vortex propagation in a nonlinear medium is the parametric frequency conversion. In this process the orbital angular momentum of the vortex beam is conserved. Thus, when the fundamental frequency (FF) beam carries an orbital angular momentum, the generated harmonic beams have to carry an orbital angular momentum as well, resulting in the generation of a *two-color optical vortex*. In the general case of the frequency mixing of two LG modes with the topological charges m_1 and m_2, the generated vortex has a topological charge of $m_3 = m_1 + m_2$ [25]. Therefore, in the parametric process such as the second-harmonic generation (SHG) the topological charge of an optical vortex should double [5, 7, 26, 27, 28]. Higher-charge vortices however, are structurally unstable and weak perturbation can initiate a decay of the second-harmonic (SH) vortex into a pair of single-charge vortices [29]. Such perturbations can arise from the spatial overlap of the first- and second-harmonic beams and the complex field gradients due to back conversion from the SH beam to the FF beam.

In typical crystals used for SHG, a variety of additional nonlinear processes, such as photorefraction, thermal focusing/defocusing, and Kerr-type self-phase modulation, can influence the nonlinear propagation of a vortex beam. When ultrashort pulses of high-peak intensities are used, the frequency conversion processes can also be accompanied by cascaded parametric [30] and higher-order nonlinear processes (e.g. self- and induced-phase modulation). The rich dynamics of such combined nonlinear interactions calls for a systematic study of the vortex dynamics in the process of SHG accompanied by the action of additional effects.

In this paper we study experimentally the nonlinear dynamics of two-color optical vortices generated in the process of non-phase matched SHG and affected by the combined effect of several different nonlinear processes such as thermal focusing, photorefractive effect, and self- and induced phase modulation. We use an iron-doped lithium niobate crystal as a nonlinear medium for the vortex propagation and observe a variety of interesting nonlinear effects including a decay of a double-charge vortex, splitting and reshaping of the background beam, pattern formation, and nonlinear rotation of the a vortex pair.

2. Experimental arrangements and parameters

In our experiments we generate OVs by passing the laser beam through a computer generated hologram (CGH) and selecting the '+1' or '-1' diffraction order after the hologram as shown in Fig. 1(top). The hologram is fabricated by etching of the corresponding vortex interference pattern onto a glass substrate. The holographic grating has a period of $80\,\mu$m and a diffraction efficiency of approximately 30% in the first order. The selected diffraction order is then focused by a lens onto an iron-doped Lithium Niobate ($LiNbO_3$) crystal with dimensions $3 \times 15 \times 20$ mm. The crystal is cut with c-axis parallel to its longest side [Fig. 1(top)]. The output of the crystal is then monitored with a CCD camera and digitized on a computer.

The $LiNbO_3$ is a negative uniaxial crystal that exhibits a combination of electro-optical, piezoelectric, pyroelectric, and photorefractive (PR) properties which makes it attractive for applications in frequency conversion [31, 32], optical modulators [33], optically-written

#91939 - $15.00 USD Received 22 Jan 2008; revised 31 Mar 2008; accepted 31 Mar 2008; published 3 Apr 2008

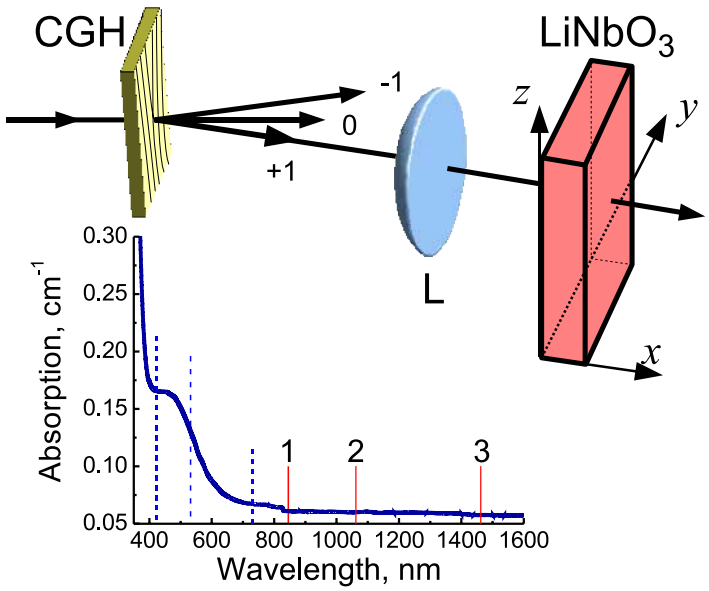

Fig. 1. Experimental arrangement (top) and absorption of the Fe:$LiNbO_3$ crystal (bottom). Solid and dashed lines indicate the FF and SH wavelengths corresponding to the three different cases in the experiment. CHG: computer generated hologram, L: focusing lens.

waveguides [34], sensors [35], and holographic recording [36, 37]. The $LiNbO_3$ is a well established optical material [38, 39] with good nonlinear properties. It is most commonly used as a medium with quadratic nonlinearity, but other effective third-order nonlinearities, including photorefractive, thermal, and pure electronic Kerr-type nonlinearity are well pronounced.

The crystalline structure of the $LiNbO_3$ is 3m thus it lacks inversion symmetry allowing the process of SHG. Obtaining proper phase matching conditions for wavelengths in the visible and near infra-red however, is practically impossible in $LiNbO_3$. For example, for degenerate phase matching of SHG at 1064 nm, temperatures of the order of -5 °C are required [40]. At other temperatures, the birefringent phase matching leads to spatial walk-off between the fundamental frequency and the second harmonic. To satisfy the phase-matching conditions in the degenerate case of propagation along the optical axis, the technique of periodic poling is exploited to ensure quasi-phase-matching. The $LiNbO_3$ appears well suitable for periodic poling and various techniques for such poling have been demonstrated [39, 41].

$LiNbO_3$ crystals doped with certain metal ions (e.g., iron or copper) exhibit enhanced photovoltaic effect at photosensitive wavelengths. The photovoltaic effect is related to photoexcitation of free electrons and their drift along the optical c-axis. The resulting space-charge field, E_{pv}, creates via electro-optic effect a nonlinear refractive index change, Δn, which is negative, saturable (as a function of light intensity), and anisotropic. When the polarization of the input light is extraordinary (along the c-axis) the largest electro-optic coefficient r_{33} contributes to the decrease of n. In this case the photorefractive index change is $\Delta n = -(1/2)n^3 r_{33} E_{pv} I/(I + I_d)$, where I, and I_d are the light intensity and dark irradiance, respectively [42, 43, 44]. The spectral sensitivity of the $LiNbO_3$ is mainly determined by the dependence of absorption on wavelength and can be approximated by the Gaussian function [45]

$$\sigma(\lambda) = \exp[-\ln(2)(\lambda - \lambda_b)^2/\lambda_w^2], \tag{1}$$

with $\lambda > \lambda_b = 400$ nm and $\lambda_w = 150$ nm.

The defocusing photovoltaic nonlinearity in $LiNbO_3$ can support vortex solitons. The first

#91939 - $15.00 USD Received 22 Jan 2008; revised 31 Mar 2008; accepted 31 Mar 2008; published 3 Apr 2008

observation of vortex self-trapping was reported in Fe-doped $LiNbO_3$ in Ref. [46].

$LiNbO_3$ also exhibits third order Kerr-type nonlinearity, which is positive and approximately three times larger than the nonlinearity of BK7 glass. For a wavelength of $1.06\,\mu$m the value of the nonlinear coefficient is $n_2 = 9.1 \times 10^{-20}$ [m^2/W] [47]. Even though this is a small value, the contribution of the Kerr nonlinearity can become appreciable when high power short laser pulses are used. The Kerr effect is mainly expressed in self-phase modulation of the pulse but, as can be seen below, can dramatically affect vortex propagation.

Due to the non-negligible absorption of our crystal in the visible and near infrared region ($400 - 800$ nm) [Fig. 1(bottom)], part of the laser beam power can be absorbed during the process of linear or two-photon absorption. The absorption of a portion of the laser power leads to heating of the sample and change of its refractive index via thermooptic effect. In the case of $LiNbO_3$ the thermooptic coefficients are $1.4 \times 10^{-6}\,K^{-1}$ for the ordinary and $39 \times 10^{-6}\,K^{-1}$ for the extraordinary polarization components, respectively at a wavelength of $1.06\,\mu$m [48]. This thermooptic effect results in an effective increase of the material refractive index and therefore self-focusing effect of the beam. The increased light intensity due to the process of thermal self-focusing on the other hand facilitates the increase of the other nonlinear effects like SHG and Kerr-nonlinearity.

The combination of different nonlinearities in $LiNbO_3$ has been studied in the terms of SHG enhancement via photorefractive soliton induced waveguides [49]. When the SH wave is generated in a crystal with non-negligible photorefraction the beam dynamics is far more rich [50]. As seen from Eq. (1), depending on the FF wavelength, λ_{FF}, the photorefraction could be initiated by the second harmonic (wavelength λ_{SH}), or to a different extent, by both the first and second harmonics. As a result, the phase matching for SHG changes in time and space. This effect appears similar to the influence of the Kerr nonlinearity on the four-wave mixing process [51, 52, 53].

In optical soliton-induced waveguides the nonlinear frequency conversion relies on phase matching between the guided modes, which have different propagation constants than the free propagating waves. This difference in propagation constants enables photorefractive tuning of the SHG process by modifying the properties of the guided modes. The first proposal of this idea (when the waveguides are induced by bright screening solitons) [54], followed by successful SHG [49] and SH wavelength tuning [55] in $KNbO_3$ was recently confirmed in $LiNbO_3$ [40]. It is also shown [56] that in Fe-doped $LiNbO_3$ crystals used in photovoltaic regime, nonlinear refractive index change originating from the second-harmonic-induced space-charge field can give rise to SH self-phase matching and effective increase of the SHG efficiency.

The experimental observation of enhanced SH in photovoltaic-dark-soliton-induced waveguide [57] is qualitatively similar to the observations with bright solitons [49, 55, 56]. In the experiment of Ref. [57] the dark soliton is created with a weak continuous-wave background laser beam with an one-dimensional odd dark stripe. Femtosecond pulse train is used as fundamental wave, while both the FF and SH radiation are able to cause photorefraction and to destroy the optically-written waveguide when the dark soliton is absent.

Here we explore a somewhat different geometry with a two-dimensional dark dislocation which is embedded already in the FF beam. In addition, we also employ three different laser sources enabling us to distinguish between different nonlinear phenomena pronounced in the $LiNbO_3$ crystal.

The parameters of the three different laser sources used in our experiments are summarized in Table 1. The lasers differ in wavelength and power, allowing us to observe independently the influence of the different nonlinear effects on vortex dynamics. In the first experiments, refereed below as *Case 1*, we use a Ti:Sapphire femtosecond oscillator (Mira 900, Coherent) emitting at a wavelength of 845 nm. In the second case, *Case 2*, a picosecond mode-locked

#91939 - $15.00 USD Received 22 Jan 2008; revised 31 Mar 2008; accepted 31 Mar 2008; published 3 Apr 2008

Table 1. Parameters of the lasers and the Fe^{3+}:$LiNbO_3$ crystal. GVM - group velocity mismatch, SOD - second order dispersion.

Laser parameters		**Case 1**	**Case 2**	**Case 3**
Wavelength	λ_{FF}, nm	845	1064	1464
Pulse duration	τ	140 fs	18 ps	150 fs
Repetition rate	f_{rep}, kHz	76 000	1500	0.25
Average power	P, mW	445	30	0.55
Peak power	P_{peak}, kW	42	1.1	15 000
Crystal parameters [38]				
Refractive index	n_o^{ω}	2.2497	2.2319	2.2139
	n_e^{ω}	2.1710	2.1556	2.1402
	$n_o^{2\omega}$	2.4076	2.3231	2.2658
	$n_e^{2\omega}$	2.3054	2.2340	2.1842
Group index	$n_o^{gr}(\omega)$	2.34259	2.29668	2.26643
	$n_e^{gr}(\omega)$	2.25102	2.21135	2.18496
	$n_o^{gr}(2\omega)$	2.91892	2.58506	2.38843
	$n_e^{gr}(2\omega)$	2.73487	2.45743	2.29041
GVM length	L_W, mm	0.10 (o-o)	26.48 (o-o)	0.52 (o-o)
		0.15 (o-e)	47.51 (o-e)	0.60 (o-e)
		0.12 (e-e)	31.03 (e-e)	2.65 (e-e)
FF SOD	SOD, fs^2	1183 (o)	821 (o)	409 (o)
		1019 (e)	712 (e)	362 (e)
FF pulse broadening	τ_{out}, fs	143 (o)	18 ps	150
		142 (e)	18 ps	150
Coherence length	L_{coh}, μm	1.57 (ee-e)	131.0 (oo-e)	8.3 (ee-e)

laser at 1064 nm was employed, and in the last case, *Case 3*, we used a Ti:Sapphire amplified system (Clark-MXR 2001) and a parametric amplifier (Light Conversion TOPAS) emitting at a wavelength of 1464 nm.

When the $LiNbO_3$ crystal is oriented with its c-axis perpendicular to the FF beam polarization (ordinary) the propagation lengths are either $l_{\text{cryst}} = 3$ mm or 15 mm [Fig. 1(top)]. The estimated pulse walk-off lengths due to group velocity mismatch (GVM) between the FF and the SH are [38] $L_W = (\tau_{FF}^2 + \tau_{SH}^2)^{1/2}/|1/V_g^{FF} - 1/V_g^{SH}|$, thus for the three lasers we have three different propagation regimes: $L_W \ll l_{\text{cryst}}$ for Case 1 ($\lambda_{FF} = 845$ nm), $L_W > l_{\text{cryst}}$ for Case 2 ($\lambda_{FF} = 1064$ nm), and $L_W \sim l_{\text{cryst}}$ for Case 3 ($\lambda_{FF} = 1464$ nm). The long L_W in Case 2 is mainly due to the longer duration of the pulse (18 ps).

The second-order dispersion (SOD) and the FF output pulse durations at the exit of the sample are estimated using refractive index data from [38] according to the relations $SOD = \lambda_0^3 l_{\text{cryst}}/(2\pi c^2)(d^2n/d\lambda^2)$. Then the pulse broadening due to SOD can be estimated as $\tau_{out} = \tau_{in}[1 + 16\ln(2)SOD^2/\tau_{in}^4]^{1/2}$ (valid in a Gaussian pulse shape approximation with τ_{in} being the input full-width pulse duration at half maximum) [58]. Our estimates for the pulse broadening (see Table 1) show that in all three cases this effect is weak and can be largely neglected.

For the process of SHG an important parameter is the coherence length, l_{coh}, defined as $l_{coh} = \pi/|\Delta k|$, where $\Delta k = 4\pi n(\omega)/\lambda_{FF} - 2\pi n(2\omega)/\lambda_{SH}$. As shown in Table 1, in all cases $l_{coh} << l_{\text{cryst}}$, therefore the process of SHG is realised under the condition of strong phase mismatch.

#91939 - $15.00 USD Received 22 Jan 2008; revised 31 Mar 2008; accepted 31 Mar 2008; published 3 Apr 2008

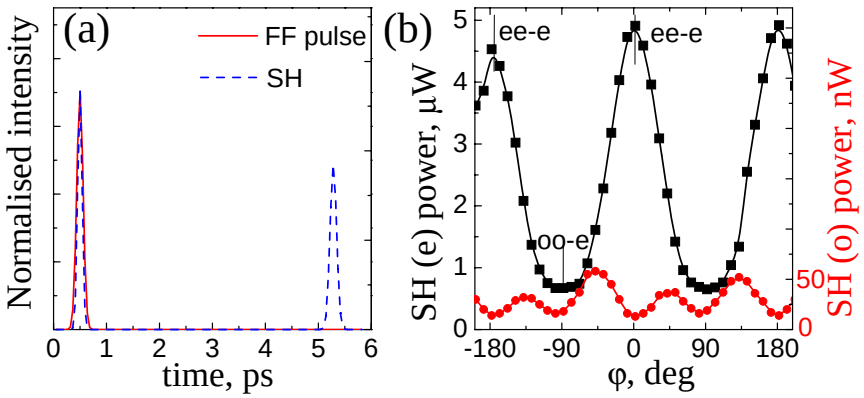

Fig. 2. (a) Calculated [64] pulse profiles of the FF (solid line) and SH (dashed line) normalized to their maximum intensity at the crystal output. (b) Average power of the ordinary and extraordinary second harmonic [SH(o) and SH(e), respectively] vs. angle of rotation of the FF beam polarization. Focusing by $f = 50$ mm lens, $l_{\mathrm{cryst}} = 3$ mm. Specific polarization components of interacting waves are marked with vertical lines. Solid lines: spline to the experimental points.

The relatively long femtosecond pulses allow us to employ a CGH for the generation of the OV beams without noticeable OV beam smearing [59, 60], pulse-front tilt [61] and associated pulse lengthening [62]. The problem of topological dispersion [63] (frequency-dependent OV topological charge) was absent as seen in Figs. 4(a,d) and the length needed to separate the desired first-order diffracted OV beam was only adjusted depending on the FF laser wavelength.

3. Case I: $\lambda_{FF} = 845$nm

3.1. *Characterization of the effective nonlinearity*

The input 140 fs pulses broaden negligibly (by $2-3$ fs) along the $LiNbO_3$ crystal for both FF wave polarizations. The GVM length is much shorter than the sample length ($l_{\mathrm{cryst}} = 3$ mm), hence the SHG at normal incidence is strongly influenced by the group-velocity mismatch. This is well expressed in Fig. 2(a) which shows the calculated [64] output pulse profiles of the FF and SH fields. The intensities are normalized to their maximal value. From the plot we see that the SH is emitted in two separate pulses [65] one of which is locked to the FF pulse and the other is delayed due to GVM.

In order to check the phase-matching conditions experimentally, we vary the FF beam polarization at the input facet of the crystal. After a polarisation filtering, the ordinary and extraordinary components [SH(o) and SH(e)] of the generated SH are recorded. The strong, nearly symmetric oscillations and the low conversion efficiency [Fig. 2(b)] are indicative for the non-phase-matched regime of the SHG. Each individual measurement in Fig. 2(b) is done at a fresh location of the crystal and at a reproducible waiting time of 2 s. According to Eq. (1) both the pump and the generated SH are able to initiate photorefraction, since the lower (three orders of magnitude) photosensitivity at the FF wavelength is compensated by the (five orders of magnitude) stronger FF intensity. In Fig. 3 we present the time evolution of the far-field FF (upper rows) and SH beam patterns (lower rows) when excited by a Gaussian FF beam. The crystal c-axis direction is vertical. Fig. 3(a) refers to a vertical (extraordinary) FF beam polarization, whereas the pictures in Fig. 3(b) are obtained with a horizontal (ordinary) FF beam polarization. Comparing the ordinary and extraordinary SH signals in Fig. 2(b), the frames in Fig. 3(a) correspond to the regime (ee-e) with dominating conversion efficiency, while these in Fig. 3(b), to

#91939 - $15.00 USD Received 22 Jan 2008; revised 31 Mar 2008; accepted 31 Mar 2008; published 3 Apr 2008

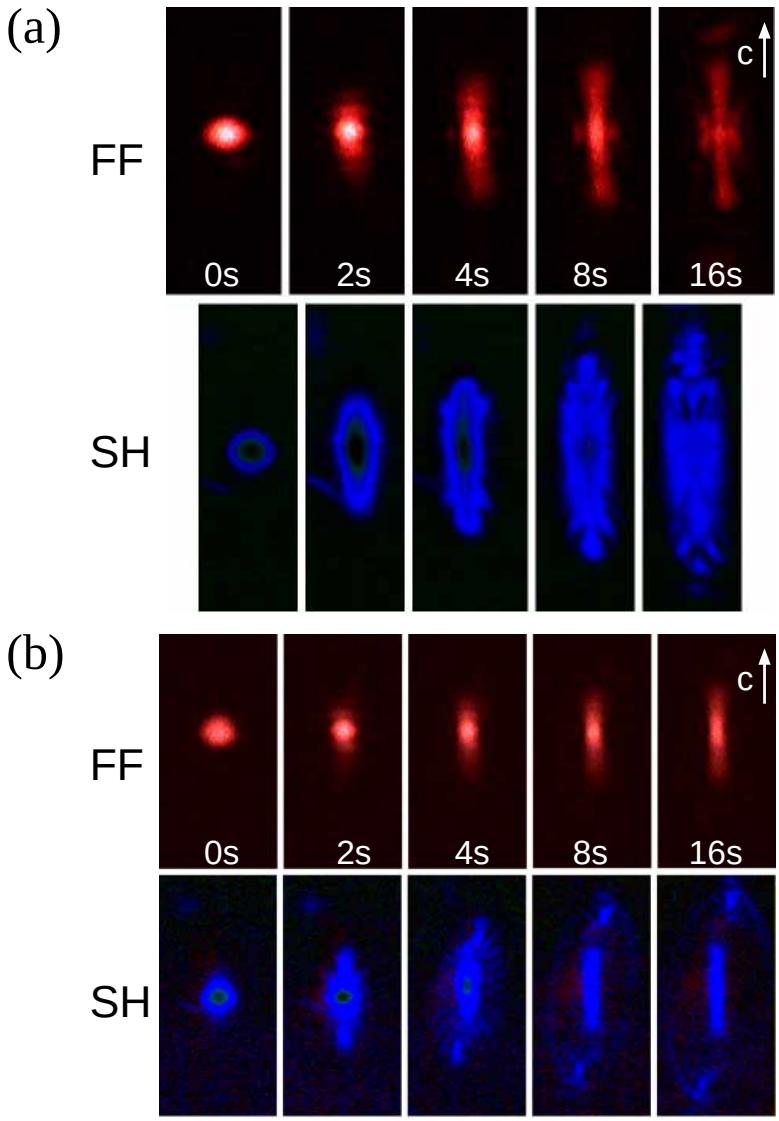

Fig. 3. Far-field FF (upper row) and SH beam patterns (lower row) vs. time: Gaussian input FF beam. Type of interaction: (a) ee-e; (b) oo-e.

(oo-e)-regime. The infrared FF beam ($\lambda_{FF} = 845\,\text{nm}$) becomes elongated along the c-axis and this is stronger pronounced for extraordinary FF beam polarization. The formation of side lobes in the FF beam in this case [see Fig. 3(a), lower row, t=16s] we explain by two mechanisms of the SH beam pattern development [56].

At the initial stage (see Fig. 3, virtual time $t = 0\,\text{s}$) the SH beam appears ring-shaped. The relatively fast (of the order of milliseconds), initial isotropic and polarization-independent response in the material indicates refractive index changes of a thermal origin [66] and results in a formation of a bright symmetric ring [not clearly visible in Fig. 3(a, 0 s)]. At this initial stage the Gaussian input FF beam also creates photorefractive carriers with symmetric distribution, however it takes longer time for these charges to separate and create space-charge field. The formation of a single bright ring at this initial stage indicates a positive refractive index

#91939 - $15.00 USD Received 22 Jan 2008; revised 31 Mar 2008; accepted 31 Mar 2008; published 3 Apr 2008

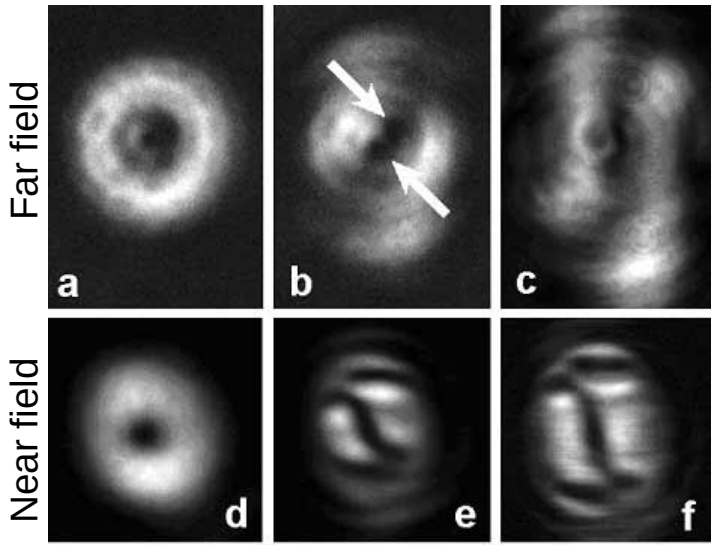

Fig. 4. SH far-field (upper row) and near field (lower row) energy density distributions of the OV beam at an initial (a,d), intermediate (b,e), and final evolution stages (c,f). The arrows indicate the position of the two vortices.

modulation $\Delta n \sim 3 \times 10^{-4}$. Later, the photorefractive nonlinearity clearly dominates, resulting in a strong asymmetry in the transverse plane and development of a complex beam structure simultaneously in the FF and SH beams. The dominating photorefractive effect also leads to a total negative index change.

When both the FF and SH waves are extraordinary [Fig. 3(a)], the strong PR nonlinearity reshapes the ring and a complex pattern is formed in the far field. The pronounced asymmetry in the $\pm$c-direction [see Fig. 3(a), lower row, $t = 16$ s] is due to the diffusion field [56].

With ordinary polarized FF waves [Fig. 3(b)], in the SH wave we observe side-lobes ($t = 2$ s) developing in a broad (of the order of the frame window, unfortunately not well visible) halo-like structure (for $t \sim 4-8$ s) surrounding the elongated (along c-axis) main part of the beam.

In summary to this subsection, in the Case 1, the nonlinear processes which accompany the SHG are the thermal positive index change at a short millisecond time scale, followed by much stronger photorefraction from both FF and SH fields on a time scale of a few seconds.

3.2. Vortex dynamics

As a next step we encode a single-charged OV in the FF beam and focus it in the middle of the $LiNbO_3$ crystal by a lens with $f = 50$ mm. As such, we obtained average SH power of $0.42\,\mu$W for extraordinary FF beam polarization at average FF power of 120 mW. In Fig. 4(upper row) we show far-field energy density distributions of the SH OV beam at an initial (a), intermediate (b), and final evolution stages (c) for a total time of approximately 30 minutes. The data are recorded with a CCD-camera build-in in a GRENOUILLE frequency-resolved optical gating device (Swamp Optics) used in a spatial mode. The same device and alignment was used to estimate that the material dispersion of the hologram substrate does not increase noticeably the FF pulse width. As seen in Fig. 4(a) the angular spreading of FF pulse spectrum ($\Delta\lambda_{FF} = 5.4$ nm) causes a negligible OV core smearing and the wings of the generated SH OV are influenced only by the diffraction. At the intermediate stage [Fig. 4(b)] one can clearly see that the double-charged SH OV is split due to the perturbation caused by the asymmetric photorefractive nonlinearity. Later, the vortex pair rotates and lines up parallel to the crystal c-axis. This effect,

#91939 - $15.00 USD Received 22 Jan 2008; revised 31 Mar 2008; accepted 31 Mar 2008; published 3 Apr 2008

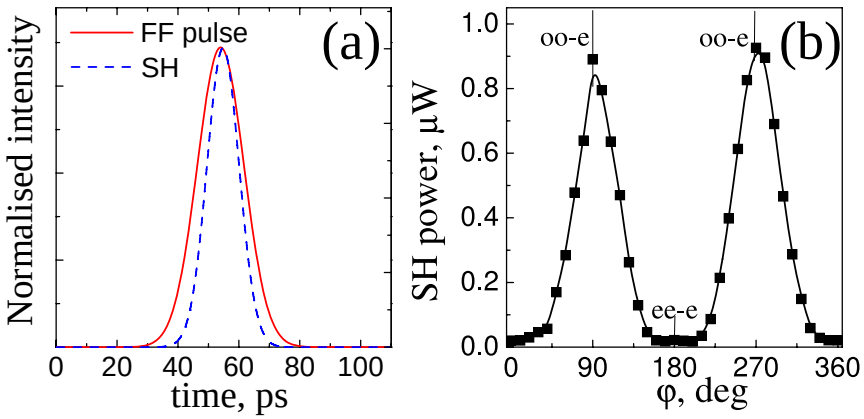

Fig. 5. (a) Calculated [64] pulse profiles of the FF (solid line) and SH (dashed line) normalized to their maximum intensity at the crystal output. (b) Average power of the extraordinary second harmonic vs. angle of rotation of the FF beam polarization. Focusing by $f = 38$ mm lens; $l_{\text{cryst}} = 3$ mm). Specific polarization components of interacting waves are marked with vertical lines. Solid line: spline to experimental points.

along with the reshaping of the FF OV beam due to the photorefraction and the dominating self- and induced defocusing along the c-axis cause the SH background beam to seemingly 'split' in two slices.

When the output of the crystal was imaged with a microscope objective ($\times 4$) onto a CCD camera [Figs. 4(d-f)] we can monitor the vortex distribution at the crystal output (near field). The recorded energy density distributions of the SH OV beam are shown in Fig. 4, lower row. As seen in Fig. 4(d), there are no signatures of diffraction reshaping and topological dispersion. The corresponding intermediate and final evolution stages are shown in Fig. 4(e) and (f), respectively. The central dark curved line is caused by the split SH OVs and the FF OV tending to line up along the sample c-axis. When the FF OV charge was reversed by rotating the CGH at 180° the SH images appeared flipped about a central vertical line, thus confirming that the observed pattern is only caused by vortex deformation and break-up.

4. Case 2: $\lambda_{FF} = 1064$nm

4.1. *Characterization of the effective nonlinearity*

For this experimental case, first we carried out benchmark measurements of the origin of the photorefraction in the crystal and its influence on the SHG phase-matching. Nonlinear self-phase matching of the SHG in $LiNbO_3$ at 1064 nm has been demonstrated with a Q-switched mode-locked laser emitting 100 ps pulses [56]. In this process, the presence of SH changes spatially the refractive index of the material, thus causing a change in the SH phase matching conditions. This change leads to improved conversion efficiency with stronger SH component resulting in a feedback self-matching mechanism. In contrast to Ref. [56], here we use a crystal oriented strictly at a normal incidence (with c-axis perpendicular to the incoming beam) and a mode-locked Nd:YVO_4 laser emitting shorter (18 ps) pulses at a repetition rate of 1.5 MHz [67]. Due to this pulse duration the generated SH pulse always overlaps with the FF pulse inside the crystal as shown in Fig. 5(a). The average power of the generated extraordinary SH at the output facet of the crystal ($l_{\text{cryst}} = 3$ mm) is shown in Fig. 5(b) as a function of the FF beam input polarization. With an input average power $P_{FF} = 30$ mW the ordinary SH always remained below 7 nW, whereas the polarization-dependent extraordinary SH showed pronounced oscillations with input polarisation and reveal that the only possible type of interaction is oo-e. Each

#91939 - $15.00 USD Received 22 Jan 2008; revised 31 Mar 2008; accepted 31 Mar 2008; published 3 Apr 2008

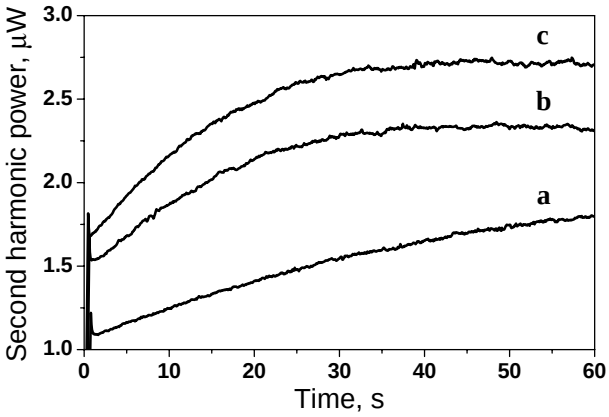

Fig. 6. Growth of the SH(e) mean power with time. Type of interaction: (oo-e). Gaussian FF beam is focused in (a) the center of the sample ($l_{\text{cryst}} = 15$ mm), on its input (b), and output facets (c) with a $f = 38$ mm AR-coated lens.

measurement is done at a fresh location of the crystal after a waiting time of 5 s.

In Fig. 6 we show the increase of the SH(e) power with time when the FF beam is focused in the center (a) of the sample, on its input (b), and output facets (c). The crystal itself was rotated to use longer beam propagation ($l_{\text{cryst}} = 15$ mm). Since only the focusing conditions are changed from curve to curve, the enhancement of the SH(e) average power with time is a clear signature of photovoltaic self-phase matching [56]. In order to determine wheatear the origin of photorefraction is coming from the FF or the SH wave, we performed a test experiment where the beam of a cw Nd:YAG laser (Coherent 1064-100) with three times higher output power (90 mW) was focused on the crystal with the same polarization. Since no signature of cw beam reshaping or fanning was observed, we are convinced that the self-phase-matching effect (Fig. 6) is due to the photovoltaic field induced by the extraordinary SH light which changes (via photorefraction) the refractive indices and phase-matching conditions. Thus for this case, we can conclude that along with the SHG process we have a strong contribution of photorefractive nonlinearity induced entirely by the SH field at 532 nm.

4.2. Vortex dynamics

As the next step, we generate an optical vortex in the FF beam and focus it onto the $LiNbO_3$ crystal with a short focal length lens $f = 38$ mm. As expected, the generated double-charge vortex in the SH field splits into a pair of two single-charge vortices, which start rotating as the photorefraction influences the refractive index. For the (oo-e) type SHG process, the SH is relatively strong, inducing strong photorefraction. As a result, the SH beam reshapes quickly breaking its symmetry, thus preventing clear identification of the angular positions of the vortices. When the input polarization is changed to 45° with respect to the c-axis [see Fig. 5(b)] the photovoltaic self-phase matching slows down keeping its monotonic and saturable character. The rotation angle of the OVs vs. time is shown in Fig. 7. The solid curve is a log-normal fit intended to guide the eye only. At the initial stage of evolution the vortex pair rotates quickly (in a few seconds) to approximately 35°, after which it continues rotating monotonically at a slower rate. The inset in Fig. 7 shows the initial ($t = 0$; left frame) and final (right frame; $t = 30$ min) orientation of the OV pair. Similar to the behavior described in Case 1, in the steady state the OVs align along the c-axis of the $LiNbO_3$ crystal.

#91939 - $15.00 USD Received 22 Jan 2008; revised 31 Mar 2008; accepted 31 Mar 2008; published 3 Apr 2008

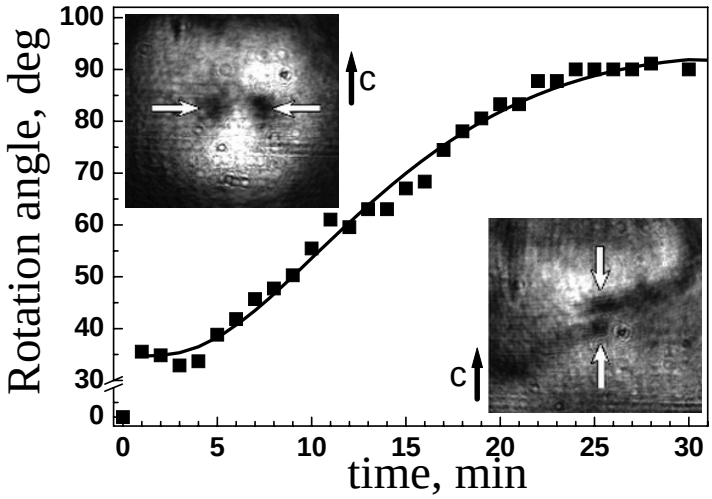

Fig. 7. Rotation of the SH(e) OV pair with time: Input polarisation at 45° with respect to the c-axis. $l_{\text{cryst}} = 15$ mm; focusing by $f = 38$ mm lens. Inset: initial (left; $t = 0$) and stationary SH pattern (right; $t = 30$ min).

5. Case 3: $\lambda_{FF} = 1464$nm

5.1. Characterization of the effective nonlinearity

In the measurements described below we use high-power pulses with the duration of 150 fs at 1464 nm and repetition rate 250 Hz. Even though in this case the average laser power is much lower, the pulse peak power is four orders of magnitude higher than in the previous two cases. The low average power and the long FF wavelength ensured that neither the FF beam nor the SH beam trigger photorefraction. Thus, in addition to the SHG process we encounter only the third-order Kerr-type nonlinearity. In this experiment we keep the $LiNbO_3$ crystal at normal incidence with respect to the laser beam ($l_{\text{cryst}} = 3$ mm) and orient it with its c-axis parallel to the FF beam polarization (ee-e type of interaction).

Unlike the previous cases, here we use an OV embedded in the FF beam even for characterisation of the nonlinearity. The input OV beam is focused by a $f = 150$ mm lens inside the $LiNbO_3$ crystal. After filtering out the FF beam, a second lens of a focal length 200 mm is used to re-collimate the SH onto a CCD camera. The lens, camera, and $LiNbO_3$ crystal are then translated together (similar to the experiments in Ref. [15]) thus varying the position of the input FF beam waist with respect to the crystal. Additionally, we can record the spectra of the SH beam exiting the crystal by a fibre spectrometer (Ocean Optics, HR2000).

In the SH spectra recorded at different positions of the $LiNbO_3$ crystal, we observe strong dependence of the SH spectral width, $\Delta\lambda$, ranging from 10.5 nm (at large waist offset, but still detectable SH) to $\Delta\lambda_{MAX} = 24.1$ nm (at the longitudinal position $z = 0$ inside the crystal). In Fig. 8(a) (solid diamonds) we show the normalized SH spectral width $\Delta\lambda/\Delta\lambda_{MAX}$ for the half of the recorded data. The reason for this spectral broadening is the third-order nonlinear process of induced-phase modulation (IPM) from the FF pulse to the SH. Due to the mild focusing of the FF beam, we can neglect the linear diffraction inside the 3 mm long crystal. Then by using the fit of the experimental data [Fig. 8(a), solid curve] and the relation $\Delta\lambda/\lambda_{MAX} \sim 1/[1+(z/L_D)]$ coming from the intensity variation in the vicinity of the FF beam waist, we can estimate the Rayleigh diffraction length $L_D = 3.6$ mm for the FF vortex beam. Since the SH wavelength is twice shorter and the SH beam radius w is expected to decrease by a factor of $\sqrt{2}$ with respect to the FF beams, this diffraction length is also a reasonable estimate for the SH beam. The dashed

#91939 - $15.00 USD Received 22 Jan 2008; revised 31 Mar 2008; accepted 31 Mar 2008; published 3 Apr 2008

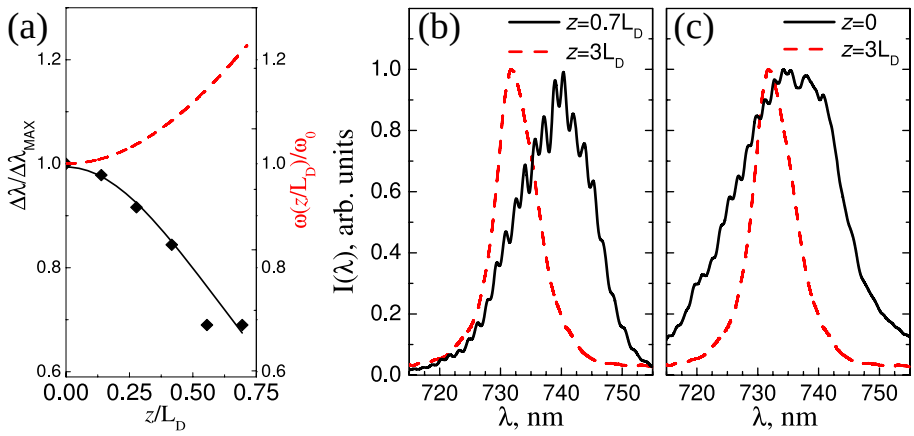

Fig. 8. (a) Normalized spectral width $\Delta\lambda(z/L_D)/\Delta\lambda_{MAX}$ of the SH pulses (diamonds – experimental data, solid curve – sigmoidal fit) and normalized FF beam spectral broadening $\omega(z/L_D)/\omega_0$ (dashed) vs. crystal position. (b,c) SH spectra of the OV pulses at different positions of the $LiNbO_3$ crystal. $\Delta\lambda_{MAX} = 24$ nm (full width at 1/e intensity level) at $x = 0$, whereas $\Delta\lambda = 17.5$ and 10.5 nm at crystal positions $z = 0.7L_D$ and $3L_D$, respectively.

curve in Fig. 8(a) visualizes the beam broadening with increasing offset of the crystal from the beam waist which decreases the FF beam intensity. The reduced intensity decreased the effect of the IPM on the SH and consequently the normalized SH spectral width $\Delta\lambda/\Delta\lambda_{MAX}$.

Since the estimated GVM length L_W (e-e) is approximately equal to the sample length and $n_e^{gr}(\omega) < n_{o,e}^{gr}(2\omega)$, the generated SH will be influenced mainly by the trailing wing of the FF pulse. Therefore, in the case of a positive third-order nonlinearity, the IPM-assisted spectral broadening has to be asymmetric. In this case one can expect an induced shift of the SH center-of-gravity wavelength (λ_c) and stronger oscillations in one of the wings of the SH spectra [68, 69]. In Fig. 8(b,c) such signatures are clearly visible when comparing the SH spectra (solid curves) recorded near [Fig. 8(b)] or at the FF beam waist [Fig. 8(c)] with the spectrum of the weak SH signal at a large offset ($x/L_D = 3$) from the FF beam waist (dashed curves). Because of the short propagation path-length in the crystal, it is unlikely that the observed red shift $\Delta\lambda_c \approx 4$ nm ($\Delta\nu \approx 74\,\mathrm{cm}^{-1}$) of the spectrum is due to the intrapulse Raman scattering [70, 71].

5.2. *Vortex dynamics*

In the spatial domain, the presence of OV in the FF beam leads to the generation of a double-charge OV in the SH beam, which splits into a pair of two OVs. The fast response of the electronic Kerr-type nonlinearity allows us to study the process of the vortex rotation (similar to Case 2), but for a positive nonlinearity and with respect to the position of the beam focusing. In Fig. 9(a) we show the retrieved angle of the rotation of an OV pair in the SH field as a function of the longitudinal position z of the crystal. The dashed curve is a sigmoidal fit intended to guide the eye only. The sequence of frames shows the far-field images recorded experimentally at the crystal positions as marked by dashed-blue circles. Despite the focusing Kerr nonlinearity, the azimuthal instability of the vortex beam [11] is not pronounced in our experiments due to a short propagation length and mild focusing inside the crystal.

In order to compare the rotation angle in the nonlinear regime with the rotation due to linear Guoy phase shift, we normalize the longitudinal coordinate to the effective Rayleigh diffraction length L_D. In this way, we can add in Fig. 9(a) the solid curve for the calculated linear Guoy phase shift at the distances of interest. For the sake of clarity one has to mention that both the GVM length L_W and the Rayleigh diffraction length L_D are comparable to the sample length

#91939 - $15.00 USD Received 22 Jan 2008; revised 31 Mar 2008; accepted 31 Mar 2008; published 3 Apr 2008

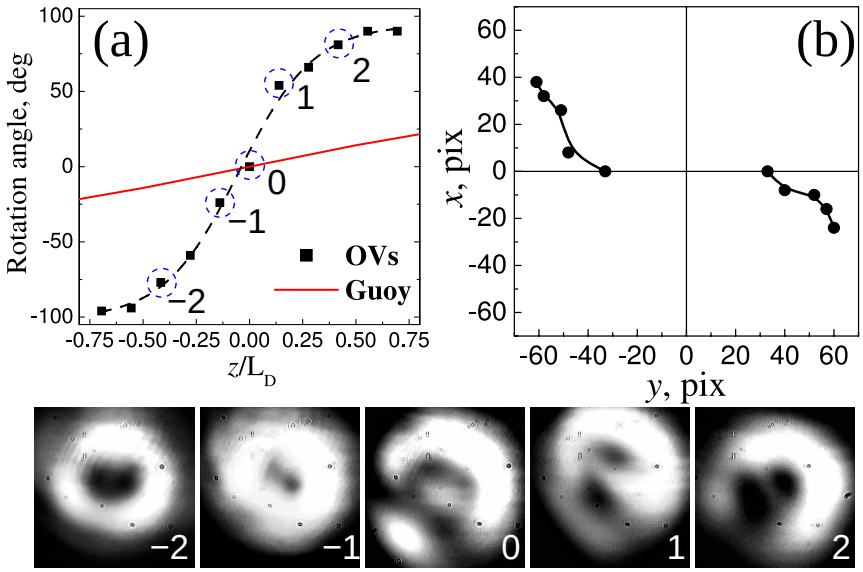

Fig. 9. (a) Rotation angle of a OV pair vs. crystal position. Squares – experimental data, dashed curve – sigmoidal fit. Solid curve – calculated rotation angle due to linear Guoy phase shift only. (b) Projection of the vortex trajectories onto the CCD camera. Lower row: experimental far-field images corresponding to the points on the graph marked with circles.

l_{cryst}. Since a significant OV rotation of $\approx 90^\circ$ is achieved over a distance $z/L_D \sim 1.5$, whereas the Gouy shift over this distance is only 40° (in agreement with Ref. [17]) the results strongly indicate a nonlinear origin of the vortex pair rotation. As seen in Fig. 9(b), the SH OVs rotation with increasing the offset of the crystal from the FF beam waist is accompanied by changes in their radial positions. To our knowledge, this is the first experimental observation of the rotation of a vortex pair due to the effect of pure Kerr-type nonlinearity.

6. Conclusions

We have presented a systematic experimental study of the nonlinear dynamics of two-color optical vortices in the presence of non-phase-matched second-harmonic generation and additional nonlinear effects of photo- and thermal refraction, self- and induced-phase modulation. We have revealed several different scenarios of the vortex evolution. When the medium is photosensitive to both the fundamental and second-harmonic wavelengths (Case 1), the different time-scales of the thermal and photovoltaic nonlinearity lead to an alignment of the two colors of the vortex beam in near field and to the generation of complex spatial patterns in far field. However, when photorefraction is initiated by the generated second-harmonic beam only (Case 2), the nonlinear self-phase matching is accompanied by rotation of a two-color vortex by 90°. Finally, we have achieved controllable vortex rotation with two-fold nonlinear increase, as well as spectral broadening of the femtosecond vortices due to the pump-induced phase modulation with possible successive femtosecond vortex pulse compression (Case 3).

Acknowledgements

The authors thank Barry Luther-Davies for a help with the laser systems and useful discussions. This work was supported by the Australian Research Council (Grant LX0666552) and the National Science Fund in Bulgaria (contract F-1303/2003). A. D. and S. S. thank the Nonlinear Physics Center of the Australian National University for a warm hospitality and support.

#91939 - $15.00 USD Received 22 Jan 2008; revised 31 Mar 2008; accepted 31 Mar 2008; published 3 Apr 2008